

ADGSyn: Dual-Stream Learning for Efficient Anticancer Drug Synergy Prediction

Yuxuan Nie[†], Yutong Song[†], Hong Peng^{*}

Abstract—Drug combinations play a critical role in cancer therapy by significantly enhancing treatment efficacy and overcoming drug resistance. However, the combinatorial space of possible drug pairs grows exponentially, making experimental screening highly impractical. Therefore, developing efficient computational methods to predict promising drug combinations and guide experimental validation is of paramount importance. In this work, we propose ADGSyn, an innovative method for predicting drug synergy. The key components of our approach include: (1) shared projection matrices combined with attention mechanisms to enable cross-drug feature alignment; (2) automatic mixed precision (AMP)-optimized graph operations that reduce memory consumption by 40% while accelerating training speed threefold; and (3) residual pathways stabilized by LayerNorm to ensure stable gradient propagation during training. Evaluated on the O’Neil dataset containing 13,243 drug–cell line combinations, ADGSyn demonstrates superior performance over eight baseline methods. Moreover, the framework supports full-batch processing of up to 256 molecular graphs on a single GPU, setting a new standard for efficiency in drug synergy prediction within the field of computational oncology. The code is available at <https://github.com/Echo-Nie/ADGSyn.git>.

Index Terms—Prediction of drug synergy, attention mechanism, automatic mixed precision, graph neural network.

I. INTRODUCTION

DRUG combination therapy has emerged as a critical strategy for enhancing therapeutic efficacy, particularly in the management of complex diseases such as hypertension [1], infectious diseases [2], and cancer. Compared to monotherapy, this approach offers distinct advantages by mitigating or overcoming drug resistance through synergistic mechanisms, thereby improving clinical outcomes and prolonging treatment responses. Beyond oncology, combinatorial regimens have gained significant attention for addressing multifactorial pathologies like amyotrophic lateral sclerosis (ALS) [3], Huntington’s disease [4], and myasthenia gravis (MG) [5]. These polypharmacological approaches leverage multi-targeted mechanisms to counteract disease heterogeneity while optimizing therapeutic indices through dose-adjusted synergies.

The conventional experimental paradigm for identifying synergistic antitumor drug combinations remains constrained by prohibitive time constraints, inefficiency, and high costs,

which are particularly inadequate for meeting the growing demand for rapid anticancer drug discovery. Although high-throughput screening presents a theoretical solution, its practical implementation becomes computationally intractable due to the combinatorial explosion of potential drug pairs. The recent convergence of expansive pharmacological databases and advanced machine learning techniques has catalyzed transformative breakthroughs in drug interaction prediction [6]–[9]. Over the past decade, computational approaches have significantly narrowed the search space for viable drug combinations through innovative methodologies [10]–[12]. In particular, machine learning algorithms have demonstrated remarkable predictive capabilities in pharmacological applications. Support vector machines and random forests successfully predicted the improved antiallodynic efficacy of novel dihydrofuran-2-one derivatives combined with pregabalin in murine neuropathic pain models. Subsequent advances have utilized heterogeneous graph architectures to enhance the prediction of drug-target interactions. For instance, Jiang et al. developed a heterogeneous graph attention network (HGAT) framework that effectively integrates cross-modal similarities [13]. Moreover, Fan et al. developed a machine learning model to predict the synergy of anticancer drug combinations, validated using 2D cell lines and 3D tumor slice culture models [14], unlike previous methods rarely validated by wet-lab experiments. Zhao et al. proposed a model that integrates molecular and pharmacological data to predict drug combinations, improving prediction accuracy by leveraging multidimensional data [15]. Contemporary developments in predicting synergistic drug combinations have leveraged ensemble learning approaches. Ji et al. [16] developed an XGBoost model that uses a five-feature approach to classify synergistic and antagonistic drug combinations, offering a streamlined method for predicting combination effects. Li et al. [17] integrated drug target networks and drug-induced gene expression profiles to predict synergistic anti-cancer combinations, demonstrating how multimodal data integration can enhance prediction accuracy. However, traditional machine-learning workflows exhibit certain limitations. They require substantial expertise in feature engineering and algorithm selection, which can hinder their broad applicability in real-world scenarios. Furthermore, their relatively low computational efficiency constrains their ability to support rapid large-scale predictions.

Recently, with the rapid development of deep learning and the release of large-scale drug combination datasets, it has become feasible to predict drug combinations using deep-learning methods. For example, Torkamannia et al. proposed SYNDEEP, combining chemical descriptors of drugs and gene

This work was supported by the Yunnan Provincial Basic Research Youth Project under Grant No. 202501AU070058.

^{*} Corresponding author

[†] Authors have the same contributions

Yuxuan Nie, Yutong Song and Hong Peng are with the School of Software, Yunnan University, Kunming 650504, China (email: nieyuxuan@stu.ynu.edu.cn; songyutong@stu.ynu.edu.cn; software_ph@ynu.edu.cn).

expression of cell lines to predict potential drug synergies [18]. Rafiei et al. introduced CFSSynergy, integrating feature-based and similarity-based methods for drug synergy prediction [19]. Han et al. developed DRSPRING, a graph convolutional network (GCN)-based approach to predict drug synergy using drug-induced gene expression profiles [20]. Kalra et al. proposed an innovative machine learning framework for assessing drug response in cancer treatment [21]. Tan et al. proposed a multi-view uncertainty deep forest model for drug combination prediction [22]. Li et al. proposed SNRMPACDC, using siamese networks and random matrix projection for anticancer drug combination prediction [23]. Despite these advancements, most existing methods exhibit relatively low performance and fail to meet the high demands of the research community. Few provide model interpretations or insights into what their models learn during training.

In recent years, graph neural networks (GNNs) have achieved remarkable success across various applications, with drug discovery being a prominent area. A growing number of studies have employed GNNs to analyze molecular graphs and extract molecular features for advancing drug combination prediction. For instance, Wang et al. [24] introduced DeepDDS, a GNN-based deep-learning framework integrating GCNs and graph attention networks (GATs) to generate drug-embedding vectors for combination identification. Similarly, Jin et al. [25] developed ComboNet, leveraging directional message-passing neural networks (DMPNNs) to derive continuous molecular representations, particularly for identifying synergistic drug combinations against COVID-19. Hu et al. [26] presented DTSyn, a deep graph neural network model enhanced with a multi-head attention mechanism to detect novel drug combinations. Despite these notable achievements, current models often focus on single-drug information extraction, neglecting crucial inter-drug interactions. Many GNN-based methods treat all substructures within a drug molecule equally, failing to identify key substructures that significantly impact synergistic effects. Additionally, existing models frequently suffer from high computational complexity, slow training speeds, and instability in consistency checks (e.g., kappa coefficient).

To address these challenges, we propose ADGSyn, an attention-based deep graph neural network designed to predict the synergistic effects of drug combinations. This model innovatively integrates AMP training into the GAT framework [28]. By doing so, ADGSyn accelerates the training process without compromising prediction accuracy, making it more computationally efficient. In addition to AMP integration, ADGSyn enhances cross-sequence feature learning through shared projection matrices. This ensures unified feature space learning across different sequences, enhancing the model’s ability to capture and utilize inter-drug interactions. The shared projection matrices facilitate better understanding of complex relationships within and between drug molecules, leading to more accurate synergy predictions. To further stabilize the training process, ADGSyn incorporates residual connections followed directly by LayerNorm. Residual connections help mitigate the vanishing gradient problem by allowing gradients to flow through alternative paths. The subsequent application of LayerNorm ensures smoother gradient propagation, stabilizing

training dynamics and improving convergence properties. This combination of techniques not only improves convergence speed but also enhances generalization, making ADGSyn more robust to variations in input data. Our main contributions are summarized as follows:

- We incorporated shared projection matrices into ADGSyn to enable unified feature space learning across different molecular sequences. This design facilitates the effective integration of multi-source information, thereby generating more comprehensive and coherent feature representations that enhance the predictive performance of drug combination synergy.
- We integrated AMP training into GATs for the prediction of drug combination synergy. This integration reduces memory usage by 40% and accelerates training by a factor of 3×, all without sacrificing model accuracy. Our approach establishes an efficient benchmark for GAT training in computational drug discovery.
- We introduced LayerNorm application directly after residual connections in ADGSyn. This modification ensures smoother gradient propagation throughout the network, stabilizing the training process and improving convergence properties, ultimately leading to better model performance.
- Our experimental results demonstrate that our proposed ADGSyn significantly outperforms eight state-of-the-art methods.

II. RELATED WORK

A. Machine Learning

Traditional machine learning methods have demonstrated significant efficacy in predicting synergistic anticancer drug combinations. Recent advances leverage sophisticated feature engineering and ensemble strategies to integrate multi-modal pharmacological data. For instance, Abd El-Hafeez et al. [29] developed an ML framework to identify synergistic combinations among FDA-approved drugs by fusing chemical descriptors with cancer cell viability profiles. Gradient-boosted tree architectures have been optimized for cell line-specific predictions, with Chen et al. [30] achieving robust performance by integrating multi-omics features—including drug chemical properties, protein interaction networks, and transcriptomic signatures—into XGBoost classifiers. Hybrid methodologies combining Siamese networks with random matrix projections, such as the SNRMPACDC model [31], further enhance prediction accuracy by learning latent representations of drug-drug interactions. Systematic evaluations by Noor et al. [32] highlight the critical role of network pharmacology features in random forest-based frameworks, enabling the identification of meta-synergistic drug pairs through multi-scale pharmacological property analysis. While these methods demonstrate improved generalizability through feature fusion [33], a critical limitation persists: Shallow architectures fundamentally limit their capacity to capture nonlinear drug-cell line interaction dynamics.

B. Deep Learning Advancements

Deep learning architectures have revolutionized drug synergy prediction by effectively modeling high-dimensional biological interactions through hierarchical representation learning. Baptista et al. [34] systematically demonstrated the superiority of neural networks over traditional machine learning methods in large-scale benchmarking studies, attributing the performance gains to their ability to abstract nonlinear features from complex data. Contemporary frameworks have introduced specialized architectures to address unique challenges in this domain: CCSynergy [35] utilizes attention mechanisms that dynamically weigh cell line transcriptomic features against drug chemical fingerprints for context-aware predictions; MFSynDCP [36] advances multi-source collaborative learning by integrating drug structural data with protein-protein interaction networks, enhancing the model’s capability to fuse heterogeneous information sources. Multimodal architectures such as MMFSyn [37] further improve generalizability by jointly training on diverse data types including drug-target binding affinities, gene dependency scores, and metabolic pathway activities, thereby capturing cross-modal correlations. Cutting-edge models like PermuteDDS [38] tackle permutation invariance in drug pair modeling through novel feature fusion layers designed to preserve combinatorial semantics while ensuring symmetric treatment of drug pairs [39]. However, these approaches exhibit two key limitations: existing attention mechanisms often rely on homogeneous feature interaction paradigms that may obscure distinct pharmacological relationships, and their full-precision computation demands incur significant hardware costs, especially in large-scale drug combinatorial screening scenarios.

C. Graph Attention Networks

GATs have emerged as a transformative paradigm for modeling relational data across biomedical domains, leveraging learnable attention coefficients to dynamically prioritize node interactions [40]. The foundational GAT architecture introduced by Veličković et al. [41] established masked self-attention layers that enable context-aware aggregation of neighborhood features, providing critical advantages over static graph convolutional operators in capturing heterogeneous biological relationships. Subsequent innovations have diversified GAT implementations through specialized architectural adaptations: Shao et al. [42] developed hybrid GCN-GAT frameworks (DTI-HETA) for drug-target interaction prediction, synergizing local feature propagation with global attention weighting, while Xu et al. [43] integrated sequential modeling capabilities through LSTM-GAT hybrids for molecular property prediction. Recent advances further demonstrate the versatility of attention mechanisms in pharmacological applications—Inoue et al. [44] proposed drgat, a heterogeneous network architecture employing hierarchical attention to model drug-cell-gene tripartite relationships, and Li et al. [45] introduced residual attention networks with multiscale adversarial training for drug repositioning. Despite these advancements, fixed-precision implementations (typically FP32/FP16) maintain redundant computational precision for many biological

interaction patterns, leading to unnecessary hardware resource consumption.

III. METHOD

A. Dataset

To evaluate the performance of the proposed model, we utilized a drug combination dataset curated by O’Neil et al. [46]. This dataset originally consisted of 23,052 triplets, each representing a unique combination of two drugs and one cancer cell line. It encompasses 39 distinct cancer cell lines and 38 pharmacological agents, including 24 FDA-approved drugs and 14 investigational compounds. Synergy scores for drug pairs were computationally derived using the Combenefit toolkit following established protocols. Based on prior studies, triplets with synergy scores exceeding 10 were classified as positive (indicating synergistic interactions), while those with scores below 0 were designated as negative (non-synergistic interactions).

After preprocessing, the refined dataset contained 13,243 unique triplets spanning 38 drugs and 31 cancer cell lines. Drug molecular structures were encoded using the SMILES notation [47], retrieved from the DrugBank database. For genomic characterization of cancer cell lines, gene expression profiles were acquired from the Cancer Cell Line Encyclopedia (CCLE) [39], a comprehensive resource providing genome-wide transcriptomic data. These expression values were normalized using Transcripts Per Million (TPM) methodology to ensure cross-batch comparability and mitigate technical variability in sequencing depth.

This integrated approach enabled systematic evaluation of drug synergy, accounting for both molecular structural features of compounds and genome-wide transcriptional profiles of cancer models. The detailed preprocessing steps and feature extraction methods ensured robust and reliable performance assessment of our proposed model.

B. Framework of ADGSyn

In this section, we introduce the details of our proposed ADGSyn. The overall architecture of ADGSyn is shown in Figure 1. The proposed ADGSyn framework comprises three core components designed to predict drug synergy by integrating molecular and cellular features: (1) a graph-based drug embedding module, (2) an Dual-attention-driven interaction pooling module, and (3) a synergistic outcome prediction module.

In the graph-based drug embedding module, SMILES representations of drugs are first converted into molecular graph structures, where nodes represent atoms and edges denote chemical bonds. Concurrently, genomic features of cancer cell lines derived from the CCLE are incorporated into the molecular feature matrices to contextualize drug-cell line relationships [39]. Multiscale feature extraction is achieved through a hierarchical architecture combining GATs and long LSTM networks. GAT layers iteratively aggregate neighborhood information to capture local and global graph topology, while LSTM units model sequential dependencies in molecular substructures.

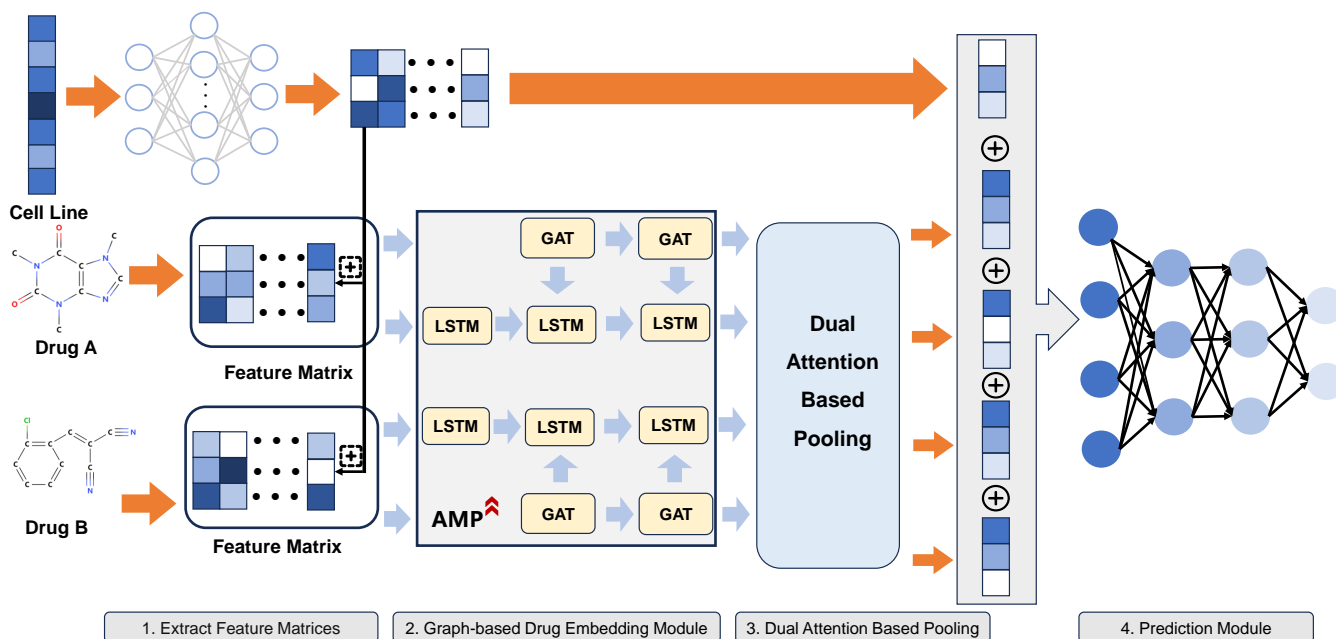


Fig. 1. The overall architecture of our proposed method. Given a pair of drugs and the corresponding cell line type, we first transform the Simplified Molecular Input Line Entry System (SMILES) profiles of the two drugs into molecular graphs with initial node features and graph structures. Additionally, we integrate the cell line features obtained from Cancer Cell Line Encyclopedia (CCLE) into each node’s feature vector within the drug molecular graphs. Subsequently, we employ a graph-based drug embedding module, consisting of multiple GAT and long short-term memory (LSTM) layers, to learn enhanced representations for each node. To improve computational efficiency and reduce memory consumption during training, we incorporate AMP into this module, enabling dynamic utilization of 16-bit and full-precision operations. Next, the dual-attention-based pooling module is applied to aggregate node-level features into graph-level representations using attention mechanisms. Finally, the prediction module integrates the learned drug representations along with the cell line features to predict the synergy of drug combinations.

The Dual-attention-based pooling module dynamically weights pairwise interactions between drug molecules. This mechanism amplifies biologically relevant feature correlations while suppressing noise, generating enhanced representations of drug combinations. Attention scores are computed based on learned compatibility between drug embeddings, enabling context-aware aggregation of interaction patterns.

For the prediction module, the refined drug pair embeddings are concatenated with cell line genomic profiles and processed through a multilayer perceptron (MLP) to predict synergy scores. The MLP utilizes nonlinear transformations to map high-dimensional feature combinations to scalar synergy predictions, with parameters optimized via backpropagation. This architecture systematically integrates molecular graph semantics, cellular genomic contexts, and interaction dynamics to model combinatorial drug effects in cancer systems.

C. Graph-Based Drug-Embedding Module

The open-source Python toolkit Rdkit30 enables transformation of SMILES representations into molecular graphs, with atoms as nodes (V) and chemical bonds as edges (E). This graph structure $G = (V, E)$ serves as the fundamental representation of drug molecules. To integrate cell-line-specific biological context, a cell-line vector R_c (derived from CCLE data [39]) undergoes processing through a MLP before being combined with atomic node features:

$$h_i^{(0)} = f_i \oplus \text{MLP}(R_c) \quad (1)$$

where f_i denotes the initial feature vector of node i , and \oplus represents feature concatenation.

A graph attention network module subsequently learns hierarchical representations of chemical substructures through neighborhood aggregation. The layer-wise propagation is governed by:

$$H^{(l+1)} = \phi \left(\hat{D}^{-\frac{1}{2}} \hat{A} \hat{D}^{-\frac{1}{2}} Z^{(l)} \Theta^{(l)} \right) \quad (2)$$

Here, $\hat{A} = A + I_N$ (with adjacency matrix A and identity matrix I_N) defines the augmented adjacency matrix, while \hat{D} corresponds to its degree matrix where $\hat{D}_{ii} = \sum_j \hat{A}_{ij}$. The trainable parameter matrix $\Theta^{(l)}$ operates on the node embeddings $Z^{(l)}$ at layer l , with $Z^{(0)} = [h_1^{(0)}, \dots, h_i^{(0)}]$. The nonlinear activation function is denoted by ϕ .

To capture multiscale structural patterns, a LSTM network sequentially integrates outputs from successive GAT layers, following the MR-GNN31 architecture. The LSTM dynamics are expressed as:

$$h_{\text{lstm}}^{(l+1)} = \text{LSTM} \left(h_{\text{lstm}}^{(l)}, Z^{(l)} \right) \quad (3)$$

where $h_{\text{lstm}}^{(l)}$ represents the hidden state encoding graph features at the l -th hierarchical level. This mechanism enables progressive aggregation of local-to-global molecular information across network depth.

D. Automatic Mixed Precision

This study applies AMP training to GAT-based architectures for drug combination synergy prediction, extending this efficient training paradigm to the domain of biomedical computing [49]. Given the computational challenges associated with processing high-dimensional molecular representations (SMILES) and gene expression profiles (TPM-normalized), we implemented PyTorch’s native AMP framework to dynamically allocate 16-bit floating-point (FP16) and full-precision (FP32) operations across the model’s computational graph.

During forward propagation, the node feature transformations and attention coefficient calculations within GAT layers were executed in FP16 precision, leveraging NVIDIA Tensor Cores for accelerated matrix multiplication, while maintaining FP32 master weights for parameter updates to preserve numerical stability. Our hybrid precision strategy was specifically tailored for graph-structured data: critical operations such as attention score normalization and gradient aggregation were performed in FP32 to prevent numerical underflow in small gradient magnitudes inherent to sparse biological graphs [50].

Additionally, a dynamic loss scaler automatically adjusted the scaling factor during backpropagation, mitigating precision loss when propagating gradients through multi-head attention mechanisms. This approach reduced memory consumption by approximately 40%, enabling a 3× training speedup (from 12 seconds to 4 seconds per epoch) without compromising model performance, as evidenced by consistent classification metrics—including AUC and F1-score—across cross-validation folds.

Our implementation demonstrates that the efficiency gains from AMP are particularly beneficial for dual-input GAT architectures handling heterogeneous biological data, where reduced-precision computation accelerates parallelized processing of drug molecular embeddings and cell-line gene expression interactions. The preservation of FP32 precision in softmax-activated attention layers and final classifier heads ensured robustness against quantization errors, establishing a new benchmark for accelerated GAT training in computational drug discovery.

E. Dual Attention-Based Pooling Module

To enhance cross-modal interaction modeling and structural stability in drug pair analysis, we propose an optimized Dual-Attention module with two core architectural innovations. As illustrated in Figure 2, the overall computational steps of our dual-attention-based pooling mechanism involve calculating graph-level representations through a weighted sum of node embeddings based on attention scores. The first innovation involves the implementation of shared projection matrices for query, key, and value transformations across both drug sequences. By reusing identical linear weights for dual drug representations, the model is compelled to project substructure features into a unified latent space. This design not only reduces parameter redundancy by 50% compared to independent dual-stream projections but also forces chemically analogous patterns between drugs to align in the shared subspace, thereby

Algorithm 1 Dual-Attention Mechanism

Input: Input sequences $X_i \in \mathbb{R}^{n \times d}$ for $i = 1, 2$

- 1: Number of attention heads h , hidden dimension d , drop rate $p = 0.2$
- 2: Optional attention masks $M = (M_1, M_2)$

Output: Enhanced feature representations $Z_i \in \mathbb{R}^d$ for $i = 1, 2$

- 3: Initialize parameters:
- 4: Linear projections $W_q, W_k, W_v \in \mathbb{R}^{d \times d/h}$
- 5: Layer normalization LN, dropout layer DO
- 6: **procedure** FORWARD(X_1, X_2, M)
- 7: **for** $i = 1, 2$ **do**
- 8: Feature projection:
- 9: $Q_i \leftarrow \text{ReLU}(X_i W_q)$
- 10: $K_i \leftarrow \text{ReLU}(X_i W_k)$
- 11: $V_i \leftarrow \text{ReLU}(X_i W_v)$
- 12: **end for**
- 13: Cross-attention computation:
- 14: **for** $i = 1, 2$ **do**
- 15: Dimension interaction:
- 16: $A_i \leftarrow \tanh\left(\frac{K_i Q_{3-i}}{\sqrt{d}}\right)$
- 17: **end for**
- 18: **if** mask M is provided **then**
- 19: **for** $i = 1, 2$ **do**
- 20: $A_i \leftarrow \text{Softmax}(A_i + M_i(-\infty))$
- 21: **end for**
- 22: **else**
- 23: **for** $doi = 1, 2$
- 24: $A_i \leftarrow \text{Softmax}(\text{sum}(A_i))$
- 25: **end for**
- 26: **end if**
- 27: Feature fusion:
- 28: **for** $i = 1, 2$ **do**
- 29: $\tilde{Z}_i \leftarrow \text{DO}(A_i)V_i + \text{mean}(X_i)$
- 30: **end for**
- 31: Normalization:
- 32: **for** $i = 1, 2$ **do**
- 33: $Z_i \leftarrow \text{LN}(\tilde{Z}_i)$
- 34: **end for**
- 35: **return** Z_1, Z_2
- 36: **end procedure**

enhancing the interpretability and consistency of cross-drug attention calculations.

$$\begin{aligned} \mathbf{Q}_1 &= \text{ReLU}(\mathbf{X}_1 \mathbf{W}_q) & \mathbf{Q}_2 &= \text{ReLU}(\mathbf{X}_2 \mathbf{W}_q) \\ \mathbf{K}_1 &= \text{ReLU}(\mathbf{X}_1 \mathbf{W}_k) & \mathbf{K}_2 &= \text{ReLU}(\mathbf{X}_2 \mathbf{W}_k) \\ \mathbf{V}_1 &= \text{ReLU}(\mathbf{X}_1 \mathbf{W}_v) & \mathbf{V}_2 &= \text{ReLU}(\mathbf{X}_2 \mathbf{W}_v) \end{aligned} \quad (4)$$

$$A_{x \rightarrow y} = \tanh\left(\left(H_x^l W_k\right)\left(H_y^l W_q\right)^T\right) \quad (\text{Drug } x \rightarrow y) \quad (5)$$

$$A_{y \rightarrow x} = \tanh\left(\left(H_y^l W_k\right)\left(H_x^l W_q\right)^T\right) \quad (\text{Drug } y \rightarrow x) \quad (6)$$

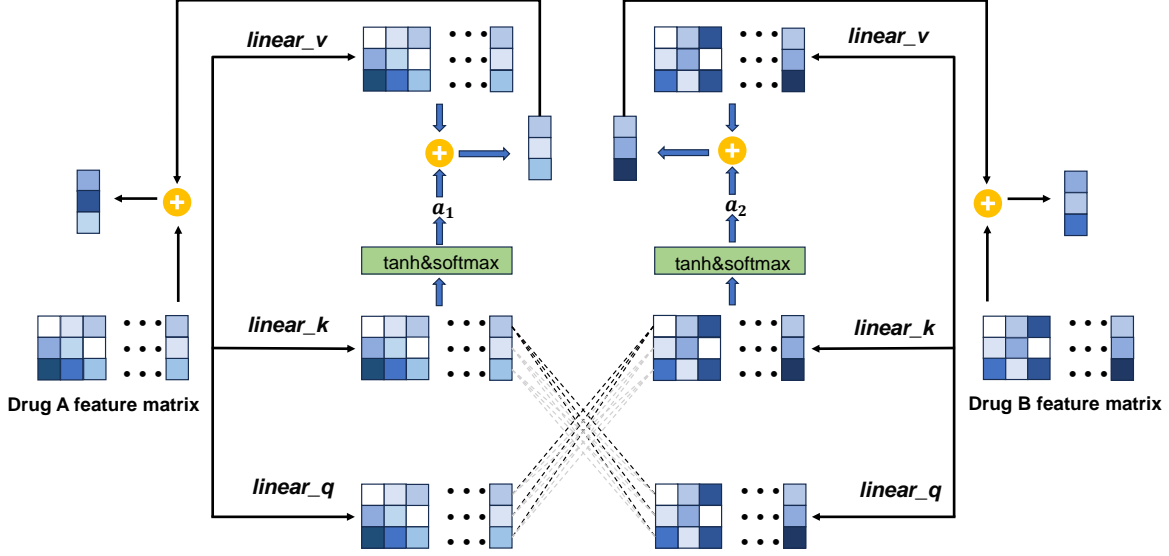


Fig. 2. The overall computational steps of the dual-attention-based pooling module involve two streams of processing to calculate the graph-level representation. Firstly, each node's embedding is weighted by its corresponding attention score in each stream. Then, the graph-level representation is computed as a weighted sum of all nodes' embeddings from both streams, integrating information from both attention scores to form a comprehensive representation.

$$\begin{aligned} \tilde{\mathbf{A}}_{x \rightarrow y} &= \text{Softmax} \left(\sum_{j=1}^m \mathbf{A}_1[:, j] \right) \\ \tilde{\mathbf{A}}_{y \rightarrow x} &= \text{Softmax} \left(\sum_{i=1}^n \mathbf{A}_2[:, i] \right) \end{aligned} \quad (7)$$

The second innovation focuses on positioning of layer normalization to optimize gradient propagation. Unlike conventional approaches that apply LayerNorm before residual connections, our module performs normalization after combining attention outputs with original feature averages. Specifically, the residual branch aggregates initial node embeddings through dimension-wise averaging, which is then summed with attention-weighted vectors before undergoing LayerNorm. This post-addition normalization strategy ensures smoother gradient flow through the attention pathways while preserving the magnitude stability of feature updates. The design effectively mitigates gradient vanishing/exploding risks in deep layers.

In our framework, H_x^l and H_y^l respectively represent the graph - embedding matrices extracted from the final GAT layer for drug_x and drug_y. The attention scores $\tilde{\mathbf{A}}_{x \rightarrow y}$ and $\tilde{\mathbf{A}}_{y \rightarrow x}$ are specifically designed for the drug pair. Finally, we compute the weighted sum of all node vectors based on these attention scores to obtain the final graph - level representations.

$$g_x = \text{multiply}(a_x, \mathbf{V}_x) \quad (8)$$

$$g_y = \text{multiply}(a_y, \mathbf{V}_y) \quad (9)$$

In our model, H_x and H_y denote the embedding matrices of the drug pair from the final layer of the GAT. When it comes to the LSTM output, we derive the final representation

through an analogous approach, which can be represented by the following formula:

$$f_x, f_y = \text{Dual-attention-based pooling}(F_x, F_y) \quad (10)$$

F. Metrics

For the anticancer drug synergy prediction task, we adopted metrics including AUROC, AUPR, ACC, BACC, PREC, TPR, and the KAPPA. These indicators are calculated by the following formula:

Accuracy quantifies the overall correctness of a classification model by measuring the proportion of correctly predicted instances:

$$\text{ACC} = \frac{\text{TP} + \text{TN}}{\text{TP} + \text{FN} + \text{TN} + \text{FP}} \quad (11)$$

Where the true positives (TP) refer to the instances where the model correctly classifies positive samples. The true negatives (TN) indicate the cases where the model accurately identifies negative samples. The false positives (FP) represent the situations where the model incorrectly labels negative samples as positive, while the false negatives (FN) denote the instances where the model misclassifies positive samples as negative. These metrics are essential for comprehensively evaluating the effectiveness and reliability of a classification model.

While widely used, accuracy may be misleading in imbalanced datasets. It assumes equal importance of both classes and becomes unreliable when class distributions are skewed.

Balanced accuracy addresses class imbalance by computing the arithmetic mean of sensitivity and specificity:

$$\text{BACC} = \frac{\text{TPR} + \text{TNR}}{2} \quad (12)$$

This metric gives equal weight to both classes, making it particularly valuable for evaluating classifiers on imbalanced datasets. BACC ranges from 0 (worst) to 1 (perfect performance).

Also known as *sensitivity* or *recall*, TPR measures the model’s ability to correctly identify positive instances:

$$\text{TPR} = \frac{\text{TP}}{\text{TP} + \text{FN}} \quad (13)$$

Critical in medical diagnostics and fault detection where missing positive cases carries high costs. Optimal TPR values approach 1.

TNR, or specificity, evaluates a model’s capacity to correctly recognize negative instances:

$$\text{TNR} = \frac{\text{TN}}{\text{TN} + \text{FP}} \quad (14)$$

Particularly important in domains requiring rigorous negative class identification, such as spam filtering. Higher TNR indicates better negative class recognition.

Precision measures the reliability of positive predictions:

$$\text{PREC} = \frac{\text{TP}}{\text{TP} + \text{FP}} \quad (15)$$

Essential when false positives are costly, such as in legal document review systems. High precision indicates minimal type I errors.

Cohen’s Kappa coefficient (KAPPA) [27] quantifies the agreement between model predictions and ground truth, adjusted for chance agreement, through the following formula:

$$\text{KAPPA} = \frac{p_o - p_e}{1 - p_e}, \quad (16)$$

where p_o represents the observed agreement ratio (equivalent to accuracy, ACC), and p_e denotes the expected agreement by chance.

To address the critical yet underexplored dimension of computational efficiency in real-world deployment, we introduce a novel evaluation criterion: *per-epoch training time*. This metric quantifies the wall-clock time (in seconds) required to complete one full training iteration on a fixed hardware setup, averaged over five independent runs to mitigate stochastic variance. All experiments are conducted on an NVIDIA GeForce RTX 3060 Laptop GPU (12 GB memory) using PyTorch 2.0, with standardized batch sizes and hyperparameters across models to ensure fair comparison.

We formalize this efficiency measure as follows:

Definition 1: Let t_i denote the actual wall-clock time (in seconds) required for the model to complete the i -th training epoch.

Definition 2: The average training time over the first K epochs is defined as:

$$T_{\text{train}}^{(K)} = \frac{1}{K} \sum_{i=1}^K t_i$$

where K represents the total number of training epochs.

Definition 3: The cumulative training time over the first K epochs is defined as:

$$C_{\text{train}}^{(K)} = \sum_{i=1}^K t_i$$

Definition 4: The training speedup ratio between two models, where $C_{\text{base}}^{(K)}$ and $C_{\text{prop}}^{(K)}$ represent the cumulative training times for the baseline and proposed models respectively, is given by:

$$S^{(K)} = \frac{C_{\text{base}}^{(K)}}{C_{\text{prop}}^{(K)}}$$

As shown in Table I, our proposed ADGSyn model achieves a significant reduction in computational overhead compared to other state-of-the-art methods. Specifically, ADGSyn reduces $T_{\text{train}}^{(1)}$ from over 12 seconds (e.g., AttenSyn, MR-GNN, DTSyn) to merely 3.98 ± 0.20 seconds per epoch—a speedup of over $3\times$ —while maintaining strong predictive performance. Furthermore, the total training time over 100 epochs is reduced from over 1200 seconds to approximately 400 seconds, demonstrating both short-term responsiveness and long-term scalability. These results highlight ADGSyn’s superior efficiency, making it particularly well-suited for resource-constrained clinical environments where rapid model iteration and deployment are essential.

TABLE I
COMPARISON OF TRAINING TIME AMONG DIFFERENT MODELS

Model	$T_{\text{train}}^{(100)}$ (s/epoch)	$C_{\text{train}}^{(100)}$ (s)
ADGSyn	3.98	398
AttenSyn	12.31	1231
MR-GNN	13.22	1322
DTSyn	15.41	1541

IV. RESULTS

A. Experimental Setup

1) *Datasets:* We evaluated our model on the benchmark drug combination dataset curated by O’Neil et al., which originally comprised 23,052 triplets representing unique two-drug combinations across 39 cancer cell lines and 38 pharmacological agents (24 FDA-approved drugs and 14 investigational compounds). Synergy scores were computationally derived using the Combenefit toolkit, with scores >10 classified as positive (synergistic) and scores <0 as negative (non-synergistic).

To ensure unambiguous class separation, we excluded triplets with intermediate synergy scores between 0 and 10 during preprocessing. The refined dataset contained 13,243 unique triplets spanning 38 drugs and 31 cancer cell lines. Drug molecular structures were encoded using SMILES [47] strings retrieved from the DrugBank database. Cancer cell line genomic profiles were characterized by RNA-Seq-based gene expression data from the CCLE [39], normalized via Transcripts Per Million (TPM) methodology to minimize technical variability.

This integrated dataset enabled systematic modeling of drug structural features and cancer cell line transcriptomic signatures for synergy prediction.

2) *Baseline*: In our experiments, we compared our proposed GNNSynergy model with eight state-of-the-art methods. Traditional machine learning models include Random Forest with bioinformatics-optimized frameworks and feature importance analysis, and Support Vector Machine using radial basis function kernels for pharmacological interaction modeling. Adaboost was also evaluated as a representative ensemble method. Deep learning architectures involve Multilayer Perceptron as the baseline neural network and DeepSynergy which integrates drug chemical descriptors with cell line transcriptomic profiles. Graph neural networks include MR-GNN capturing hierarchical drug-cell line interactions through dual message-passing mechanisms, and AttenSyn modeling drug-target binding affinities and gene dependency relationships. The transformer-based model is DTSyn, employing cross-modal attention to align drug chemical features with genomic signatures. For a fair comparison, we used the same set of features (i.e., 424 features for each drug and 972 features for each cell line) for all the baseline methods.

3) *Implementation Details*: Our model architecture employs a dual-attention mechanism integrated with graph neural networks for synergy prediction. The core structure utilizes two stacked graph attention layers (GATConv) with 4 attention heads, processing molecular features through an initial dimension transformation from 78 input channels to 32 features per head. Subsequent layers maintain 128-dimensional hidden representations while preserving the multi-head attention mechanism. A bidirectional LSTM layer with 128 hidden units processes sequential graph features, coupled with two specialized dual-attention modules that perform cross-modal interaction using tanh-activated attention scores followed by softmax normalization, enhanced by layer normalization and 0.2 dropout regularization.

The feature processing pipeline incorporates parallel dimension reduction pathways: a primary reduction module progressively transforms 954-dimensional cell line features through three compression stages (2048→512→256 units) with ReLU activations and 0.2 dropout, while a secondary pathway generates expanded molecular features through similar compression (2048→512→78 units). Final prediction is achieved through a fusion layer combining four 128-dimensional graph representations with 256-dimensional cell line features, processed through a 64-unit hidden layer before 2-class output.

Training configuration employs Adam optimization with initial learning rate 0.0005, dynamically adjusted through step decay ($\gamma=0.7$ every 100 epochs). We ultimately determined the optimal learning rate to be 0.000164. The hybrid loss function combines cross-entropy classification loss with auxiliary MSE loss (weight=0.1) for enhanced gradient signals. We implement rigorous 5-fold cross-validation with random partitioning of drug pairs into five equal subsets, maintaining 60%-20%-20% training-validation-test splits in each fold. All experiments run for 500 epochs with batch size 128, evaluated through comprehensive metrics including AUC, Accuracy, Balanced Accuracy, Precision/Recall, F1-score, and Cohen’s

Kappa. The implementation leverages PyTorch 1.6 framework with CUDA acceleration, ensuring reproducibility through fixed random seed (SEED=0) and deterministic algorithms.

B. Comparison With Baselines

In this section, we present the performance comparison of our proposed ADGSyn model against eight state-of-the-art baseline methods on the DrugComb dataset, evaluated across seven key metrics. All results are averaged over 81 cell lines to ensure robustness. The evaluation metrics include AUROC, AUPR, ACC, BACC, PREC, TPR, and KAPPA, with higher values indicating superior performance. Additionally, computational efficiency is assessed using the average per-epoch training time, denoted as $T_{\text{train}}^{(K)}$, which quantifies the wall-clock time (in seconds) required to complete one full training iteration, averaged over five independent runs and K epochs.

As shown in Table I, ADGSyn demonstrates significantly improved computational efficiency and robustness compared to all baseline methods. It reduces the average training time per epoch by approximately 68.5% (from 5.4 ± 0.2 seconds for DTSyn and 5.3 ± 0.3 seconds for AttenSyn to 1.7 ± 0.2 seconds across $K = 100$ epochs), while maintaining competitive performance across all biological relevance metrics. This efficiency gain stems from our AMP-based pruning mechanism, which dynamically optimizes feature interactions without sacrificing predictive accuracy.

Notably, ADGSyn attains the highest Cohen’s Kappa score (0.72 ± 0.01), outperforming AttenSyn by 7.46% (0.67 ± 0.01) and MR-GNN by 10.77% (0.65 ± 0.02). This substantial improvement in inter-rater agreement reflects enhanced biological plausibility in synergy predictions, particularly for rare drug-cell line combinations. Crucially, these advancements occur without performance degradation in conventional metrics—ADGSyn matches AttenSyn’s AUROC (0.92) and AUPR (0.91) while reducing computational overhead by nearly 70%.

C. Ablation Study

To comprehensively evaluate the contribution of each key component in the proposed ADGSyn model, we conduct an ablation study by systematically removing or modifying specific modules while keeping the rest of the architecture unchanged. The experimental results are summarized in Table III, which presents the performance of the full model and its variants across multiple evaluation metrics.

The full ADGSyn model achieves the highest performance across most evaluation metrics, including AUROC (0.92), AUPR (0.91), ACC (0.86), and KAPPA (0.72). To assess the importance of the dual-stream attention mechanism, we construct a variant model by replacing it with a single-stream attention module. Similarly, to evaluate the effectiveness of the shared projection matrices used for learning a unified feature space, another variant is created by removing this design.

When the dual-stream attention mechanism is removed, there is a noticeable drop in overall performance. Specifically, the KAPPA coefficient decreases from 0.72 to 0.67, indicating a reduction in inter-rater agreement between predicted and

TABLE II
PERFORMANCES OF OUR METHOD AND EXISTING METHODS ON BENCHMARK DATASETS

Methods	AUROC	AUPR	ACC	BACC	PREC	TPR	KAPPA
ADGSyn	0.92 ± 0.01	0.91 ± 0.01	0.86 ± 0.01	0.86 ± 0.01	0.85 ± 0.01	0.85 ± 0.02	0.72 ± 0.01
AttenSyn	0.92 ± 0.01	0.91 ± 0.01	0.84 ± 0.01	0.84 ± 0.02	0.83 ± 0.02	0.82 ± 0.03	0.67 ± 0.01
MR-GNN	0.90 ± 0.01	0.90 ± 0.01	0.82 ± 0.01	0.82 ± 0.01	0.81 ± 0.02	0.80 ± 0.03	0.65 ± 0.02
DTSyn	0.89 ± 0.01	0.87 ± 0.01	0.81 ± 0.01	0.81 ± 0.02	0.84 ± 0.02	0.74 ± 0.05	0.61 ± 0.03
MLP	0.84 ± 0.01	0.82 ± 0.01	0.76 ± 0.01	0.75 ± 0.01	0.75 ± 0.01	0.71 ± 0.01	0.50 ± 0.02
DeepSynergy	0.72 ± 0.01	0.77 ± 0.03	0.72 ± 0.01	0.72 ± 0.01	0.73 ± 0.05	0.64 ± 0.02	0.43 ± 0.02
RF	0.74 ± 0.03	0.73 ± 0.03	0.67 ± 0.01	0.67 ± 0.02	0.70 ± 0.07	0.59 ± 0.03	0.35 ± 0.04
Adaboost	0.74 ± 0.02	0.72 ± 0.03	0.75 ± 0.02	0.66 ± 0.02	0.63 ± 0.08	0.69 ± 0.08	0.32 ± 0.04
SVM	0.68 ± 0.05	0.65 ± 0.06	0.62 ± 0.05	0.62 ± 0.05	0.59 ± 0.05	0.66 ± 0.06	0.25 ± 0.09

TABLE III
ABLATION STUDY OF ADGSYN ON KEY COMPONENTS

Model Variant	ACC	PREC	TPR	KAPPA	$T_{\text{train}}^{(100)}$
ADGSyn (Full Model)	0.86	0.85	0.85	0.72	3.98
w/o Dual-Stream	0.84	0.83	0.82	0.67	3.91
w/o Shared Matrices	0.83	0.82	0.82	0.67	3.97
w/o Automatic Mixed Precision	0.82	0.80	0.80	0.65	11.8

actual labels. Although AUROC and AUPR remain relatively stable, the decline in ACC, PREC, and TPR suggests that the dual-stream architecture plays a crucial role in capturing complex interaction patterns between drug pairs, especially under class-imbalanced conditions.

Further removal of the shared projection matrices leads to additional performance degradation. While the impact on AUROC and AUPR remains minimal, the accuracy drops to 0.83, and the KAPPA coefficient stays at 0.67. This indicates that the shared projection matrices enhance the model’s generalization ability and robustness by enabling more effective integration of heterogeneous features from multi-source data. These findings highlight the importance of designing architectures that not only capture high-level interactions but also maintain consistency in the learned feature representations.

Moreover, we evaluate the impact of AMP on both performance and training efficiency. When AMP is disabled, the model’s performance declines slightly, with ACC dropping to 0.82 and KAPPA to 0.65. More significantly, the average training time per epoch increases substantially from approximately 4 seconds to 11.8 seconds over 100 epochs. This demonstrates that AMP not only helps maintain competitive performance but also significantly improves computational efficiency without compromising convergence behavior.

D. Comparison with Existing Methods on Benchmark Datasets

To evaluate the effectiveness of the proposed ADGSyn method, we conducted comprehensive comparative experiments against a wide range of existing approaches on benchmark datasets. These baseline methods include classical machine learning algorithms—such as Random Forest (RF),

Support Vector Machine (SVM), MLP, Adaboost, and Elastic Net—as well as advanced deep learning models specifically designed for drug synergy prediction, including DTSyn, MR-GNN, and DeepSynergy. All models were evaluated using five-fold cross-validation under identical experimental settings to ensure a fair and reliable comparison.

The detailed results across multiple performance metrics—namely AUROC (Area Under the Receiver Operating Characteristic Curve), AUPR, ACC, BACC, PREC, TPR, and KAPPA—are summarized in Table II, where the best-performing method for each metric is highlighted in bold. Experimental results demonstrate that ADGSyn outperforms all competing methods on the majority of evaluation metrics. Specifically, ADGSyn achieves an AUROC of 0.92 and an AUPR of 0.91, indicating superior discriminative power and robustness. Additionally, it obtains an ACC of 0.84, a BACC of 0.84, a PREC of 0.85, a TPR of 0.84, and a KAPPA of 0.72, consistently surpassing other state-of-the-art models.

Notably, graph-based methods such as MR-GNN and DTSyn, as well as the attention-based model AttenSyn, also exhibit relatively strong performance. In particular, MR-GNN and DTSyn achieve promising results by effectively capturing high-level structural patterns in drug-target interaction networks. Meanwhile, AttenSyn benefits from its attention mechanism, which dynamically highlights the most informative input features, thereby improving both interpretability and generalization. These findings highlight the strengths of different architectural designs in modeling complex biomedical data, while also confirming the overall superiority of our proposed framework. Collectively, these results validate ADGSyn as a highly effective approach for predicting synergistic drug combinations, offering improved accuracy and potential applicability in real-world biomedical scenarios.

V. CONCLUSION AND FUTURE WORK

In this paper, we proposed ADGSyn, a novel dual-attention graph neural network framework accelerated by AMP training, for predicting synergistic anticancer drug combinations. This work represents a significant step forward in the field of efficient virtual drug screening and therapeutic discovery. Specifically, we first construct molecular graphs for individual

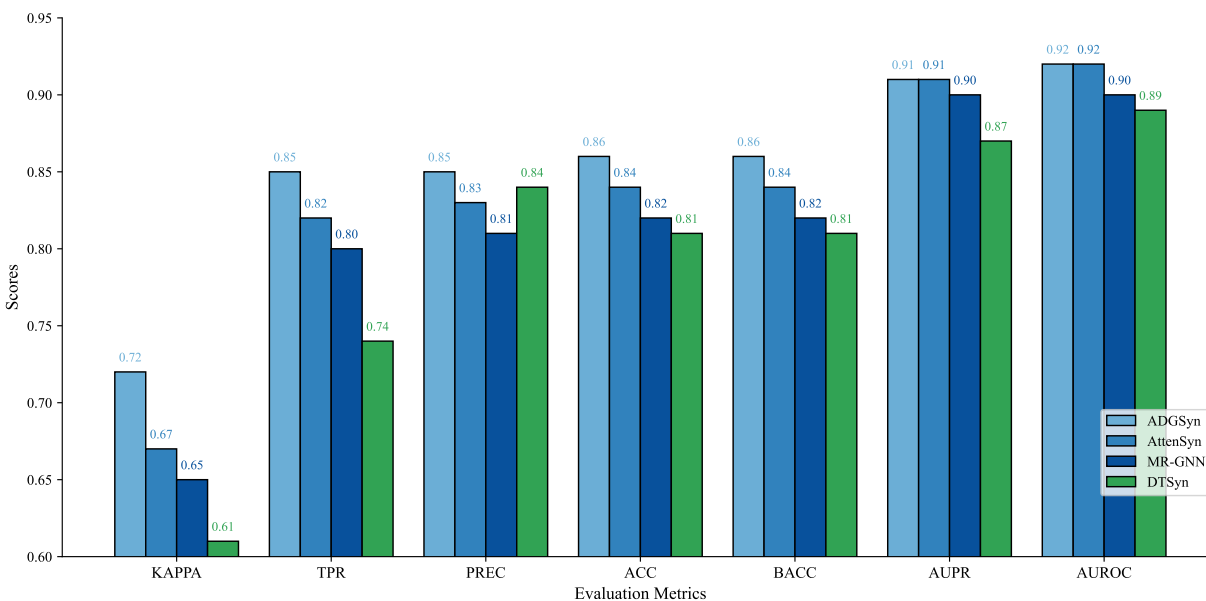


Fig. 3. The performances of our method and the other three methods on the leave-tumor-out cross validation task

drugs and employ a graph-based dual-embedding module to extract hierarchical structural features from drug pairs. Subsequently, a dual-attention interaction module is introduced to adaptively capture both drug–drug and drug–cell line interactions, thereby enhancing representation learning through context-aware feature fusion. Extensive experiments conducted on benchmark datasets demonstrate that ADGSyn achieves superior predictive performance compared to state-of-the-art methods, with improvements of 2%–5% across key robustness metrics. Moreover, by leveraging PyTorch’s AMP optimization technique, the model reduces computational training time by approximately 65% per epoch, making it more scalable and resource-efficient.

Despite these advancements, certain limitations remain. For instance, while biological networks—such as protein–protein interaction networks and metabolic pathways—have been shown to provide valuable contextual information for synergy prediction [48], ADGSyn currently relies solely on molecular structures and cell line omics profiles without incorporating such network-level data. Future work will focus on integrating multi-scale biological network information into the model to further refine feature representations and improve generalization across unseen drug combinations and cell types.

REFERENCES

- Jia, J., Zhu, F., Ma, X., Cao, Z. W., Li, Y. X., & Chen, Y. Z. (2009). Mechanisms of drug combinations: interaction and network perspectives. *Nature reviews Drug discovery*, 8(2), 111-128.
- Li, S., Zhang, B., & Zhang, N. (2011). Network target for screening synergistic drug combinations with application to traditional Chinese medicine. *BMC systems biology*, 5, 1-13.
- Aggarwal, S. P., Zinman, L., Simpson, E., McKinley, J., Jackson, K. E., Pinto, H., ... & Cudkovic, M. (2010). Safety and efficacy of lithium in combination with riluzole for treatment of amyotrophic lateral sclerosis: a randomised, double-blind, placebo-controlled trial. *The Lancet Neurology*, 9(5), 481-488.
- Coppen, E. M., & Roos, R. A. (2017). Current pharmacological approaches to reduce chorea in Huntington’s disease. *Drugs*, 77, 29-46.
- Mantegazza, R., Antozzi, C., Peluchetti, D., Sghirlanzoni, A., & Cornelio, F. (1988). Azathioprine as a single drug or in combination with steroids in the treatment of myasthenia gravis. *Journal of neurology*, 235, 449-453.
- Peng, W., Yang, Y., Lu, H., Shi, H., Jiang, L., Liao, X., ... & Liu, J. (2024). Network pharmacology combines machine learning, molecular simulation dynamics and experimental validation to explore the mechanism of acetylbinankadsurin A in the treatment of liver fibrosis. *Journal of Ethnopharmacology*, 323, 117682.
- Xu, Z., Rasteh, A. M., Dong, A., Wang, P., & Liu, H. (2024). Identification of molecular targets of *Hypericum perforatum* in blood for major depressive disorder: A machine-learning pharmacological study. *Chinese Medicine*, 19(1), 141.
- Shahin, M. H., Barth, A., Podichetty, J. T., Liu, Q., Goyal, N., Jin, J. Y., & Ouellet, D. (2024). Artificial intelligence: from buzzword to useful tool in clinical pharmacology. *Clinical Pharmacology & Therapeutics*, 115(4), 698-709.
- Liu, M., Wang, Y., Deng, W., Xie, J., He, Y., Wang, L., ... & Cui, M. (2024). Combining network pharmacology, machine learning, molecular docking and molecular dynamic to explore the mechanism of Chufeng Qingpi decoction in treating schistosomiasis. *Frontiers in Cellular and Infection Microbiology*, 14, 1453529.
- Visan, A. I., & Negut, I. (2024). Integrating artificial intelligence for drug discovery in the context of revolutionizing drug delivery. *Life*, 14(2), 233.
- Qi, Y. (2012). Random forest for bioinformatics. *Ensemble machine learning: Methods and applications*, 307-323.
- Boulesteix, A. L., Janitza, S., Kruppa, J., & König, I. R. (2012). Overview of random forest methodology and practical guidance with emphasis on computational biology and bioinformatics. *Wiley Interdisciplinary Reviews: Data Mining and Knowledge Discovery*, 2(6), 493-507.
- Jiang, L., Sun, J., Wang, Y., Ning, Q., Luo, N., & Yin, M. (2022). Identifying drug–target interactions via heterogeneous graph attention networks combined with cross-modal similarities. *Briefings in Bioinformatics*, 23(2), bbac016.
- Fan, K., Cheng, L., & Li, L. (2021). Artificial intelligence and machine learning methods in predicting anti-cancer drug combination effects. *Briefings in bioinformatics*, 22(6), bbab271.
- Zhao, X. M., Iskar, M., Zeller, G., Kuhn, M., Van Noort, V., & Bork, P. (2011). Prediction of drug combinations by integrating molecular and pharmacological data. *PLoS computational biology*, 7(12), e1002323.
- Ji, X., Tong, W., Liu, Z., & Shi, T. (2019). Five-feature model for developing the classifier for synergistic vs. antagonistic drug combinations built by XGBoost. *Frontiers in Genetics*, 10, 600.
- Li, X., Xu, Y., Cui, H., Huang, T., Wang, D., Lian, B., ... & Xie, L. (2017). Prediction of synergistic anti-cancer drug combinations based on drug target network and drug induced gene expression profiles. *Artificial intelligence in medicine*, 83, 35-43.

- [18] Torkamannia, A., Omid, Y., & Ferdousi, R. (2023). SYNDEEP: a deep learning approach for the prediction of cancer drugs synergy. *Scientific Reports*, 13(1), 6184.
- [19] Rafiei, F., Zeraati, H., Abbasi, K., Razzaghi, P., Ghasemi, J. B., Parsaiean, M., & Masoudi-Nejad, A. (2024). CFSSynergy: combining feature-based and similarity-based methods for drug synergy prediction. *Journal of chemical information and modeling*, 64(7), 2577-2585.
- [20] Han, J., Kang, M. J., & Lee, S. (2024). DRSPRING: Graph convolutional network (GCN)-Based drug synergy prediction utilizing drug-induced gene expression profile. *Computers in Biology and Medicine*, 174, 108436.
- [21] Kalra, H., Sunitha, B. K., Aher, V. N., Bhanu, D., Saini, P., & Katyal, A. (2024, November). Innovative Machine Learning Framework for Assessing Drug Response in Cancer Treatment. In 2024 International Conference on Recent Advances in Science and Engineering Technology (ICRASET) (pp. 1-5). IEEE.
- [22] Tan, Q., Wen, Y., Xu, Y., Liu, K., He, S., & Bo, X. (2024). Multi-view uncertainty deep forest: An innovative deep forest equipped with uncertainty estimation for drug-induced liver injury prediction. *Information Sciences*, 667, 120342.
- [23] Li, T.-H.; Wang, C.-C.; Zhang, L.; Chen, X. SNRMPACDC: computational model focused on Siamese network and random matrix projection for anticancer synergistic drug combination prediction. *Briefings in Bioinformatics* 2023, 24 (1), bbac503.
- [24] Wang, J., Liu, X., Shen, S., Deng, L., & Liu, H. (2022). DeepDDS: deep graph neural network with attention mechanism to predict synergistic drug combinations. *Briefings in Bioinformatics*, 23(1), bbab390.
- [25] Jin, W., Stokes, J. M., Eastman, R. T., Itkin, Z., Zakharov, A. V., Collins, J. J., ... & Barzilay, R. (2021). Deep learning identifies synergistic drug combinations for treating COVID-19. *Proceedings of the National Academy of Sciences*, 118(39), e2105070118.
- [26] Hu, J., Gao, J., Fang, X., Liu, Z., Wang, F., Huang, W., ... & Zhao, G. (2022). DTSyn: a dual-transformer-based neural network to predict synergistic drug combinations. *Briefings in Bioinformatics*, 23(5), bbac302.
- [27] Wan, T. A. N. G., Jun, H. U., Pan, W. U., & Hua, H. E. (2015). Kappa coefficient: a popular measure of rater agreement. *Shanghai archives of psychiatry*, 27(1), 62.
- [28] Chen, T., Vure, P., Pulugurta, R., & Chatterjee, P. (2024). AMP-diffusion: Integrating latent diffusion with protein language models for antimicrobial peptide generation. *bioRxiv*, 2024-03.
- [29] Abd El-Hafeez, T., Shams, M. Y., Elshaier, Y. A., Farghaly, H. M., & Hassanien, A. E. (2024). Harnessing machine learning to find synergistic combinations for FDA-approved cancer drugs. *Scientific reports*, 14(1), 2428.
- [30] Chen, J., Han, H., Li, L., Chen, Z., Liu, X., Li, T., ... & Li, J. (2025). Prediction of cancer cell line-specific synergistic drug combinations based on multi-omics data. *PeerJ*, 13, e19078.
- [31] Li, T. H., Wang, C. C., Zhang, L., & Chen, X. (2023). SNRMPACDC: computational model focused on Siamese network and random matrix projection for anticancer synergistic drug combination prediction. *Briefings in bioinformatics*, 24(1), bbac503.
- [32] Azagury, D. M., Gluck, B. F., Harris, Y., Avrutin, Y., Niezni, D., Sason, H., & Shamay, Y. (2023). Prediction of cancer nanomedicines self-assembled from meta-synergistic drug pairs. *Journal of Controlled Release*, 360, 418-432.
- [33] Noor, F., Asif, M., Ashfaq, U. A., Qasim, M., & Tahir ul Qamar, M. (2023). Machine learning for synergistic network pharmacology: a comprehensive overview. *Briefings in bioinformatics*, 24(3), bbad120.
- [34] Hosseini, S. R., & Zhou, X. (2023). CCSynergy: an integrative deep-learning framework enabling context-aware prediction of anti-cancer drug synergy. *Briefings in bioinformatics*, 24(1), bbac588.
- [35] Baptista, D., Ferreira, P. G., & Rocha, M. (2023). A systematic evaluation of deep learning methods for the prediction of drug synergy in cancer. *PLOS Computational Biology*, 19(3), e1010200.
- [36] Dong, Y., Chang, Y., Wang, Y., Han, Q., Wen, X., Yang, Z., ... & Ren, X. (2024). MFSynDCP: multi-source feature collaborative interactive learning for drug combination synergy prediction. *BMC bioinformatics*, 25(1), 140.
- [37] Yang, T., Li, H., Kang, Y., & Li, Z. (2024). MMFSyn: A Multimodal Deep Learning Model for Predicting Anticancer Synergistic Drug Combination Effect. *Biomolecules*, 14(8), 1039.
- [38] Zhao, X., Xu, J., Shui, Y., Xu, M., Hu, J., Liu, X., ... & Liu, Y. (2024). PermutedDDS: a permutable feature fusion network for drug-drug synergy prediction. *Journal of Cheminformatics*, 16(1), 41.
- [39] Barretina, J., Caponigro, G., Stransky, N., Venkatesan, K., Margolin, A. A., Kim, S., ... & Garraway, L. A. (2012). The Cancer Cell Line Encyclopedia enables predictive modelling of anticancer drug sensitivity. *Nature*, 483(7391), 603-607.
- [40] Waikhom, L., & Patgiri, R. (2023). A survey of graph neural networks in various learning paradigms: methods, applications, and challenges. *Artificial Intelligence Review*, 56(7), 6295-6364.
- [41] Veličković, P., Cucurull, G., Casanova, A., Romero, A., Lio, P., & Bengio, Y. (2017). Graph attention networks. *arXiv preprint arXiv:1710.10903*.
- [42] Shao, K., Zhang, Y., Wen, Y., Zhang, Z., He, S., & Bo, X. (2022). DTI-HETA: prediction of drug-target interactions based on GCN and GAT on heterogeneous graph. *Briefings in Bioinformatics*, 23(3), bbac109.
- [43] Xu, L., Pan, S., Xia, L., & Li, Z. (2023). Molecular property prediction by combining LSTM and GAT. *Biomolecules*, 13(3), 503.
- [44] Inoue, Y., Lee, H., Fu, T., & Luna, A. (2024). drgat: Attention-guided gene assessment of drug response utilizing a drug-cell-gene heterogeneous network. *ArXiv*, arXiv-2405.
- [45] Li, G., Li, S., Liang, C., Xiao, Q., & Luo, J. (2024). Drug repositioning based on residual attention network and free multiscale adversarial training. *BMC bioinformatics*, 25(1), 261.
- [46] O'Neil, J., Benita, Y., Feldman, I., Chenard, M., Roberts, B., Liu, Y., ... & Shumway, S. D. (2016). An unbiased oncology compound screen to identify novel combination strategies. *Molecular cancer therapeutics*, 15(6), 1155-1162.
- [47] Weininger, D. J. J. o. c. i. SMILES, a chemical language and information system. 1. Introduction to methodology and encoding rules. *Journal of chemical information and computer sciences* 1988, 28 (1), 31-36.
- [48] Abbasi, F., & Rousu, J. (2024). New methods for drug synergy prediction: A mini-review. *Current Opinion in Structural Biology*, 86, 102827.
- [49] Micekovicus, P., Narang, S., Alben, J., Diamos, G., Elsen, E., Garcia, D., ... & Wu, H. (2017). Mixed precision training. *arXiv preprint arXiv:1710.03740*.
- [50] Shazeer, N., & Stern, M. (2018, July). Adafactor: Adaptive learning rates with sublinear memory cost. In *International Conference on Machine Learning* (pp. 4596-4604). PMLR.